Supporting Information

Double redox aqueous capacitor with high energy output

Adam Slesinski, Sylwia Sroka, Sergio Aina, Justyna Piwek, Krzysztof Fic,

Maria Pilar Lobera, Maria Bernechea, Elzbieta Frackowiak

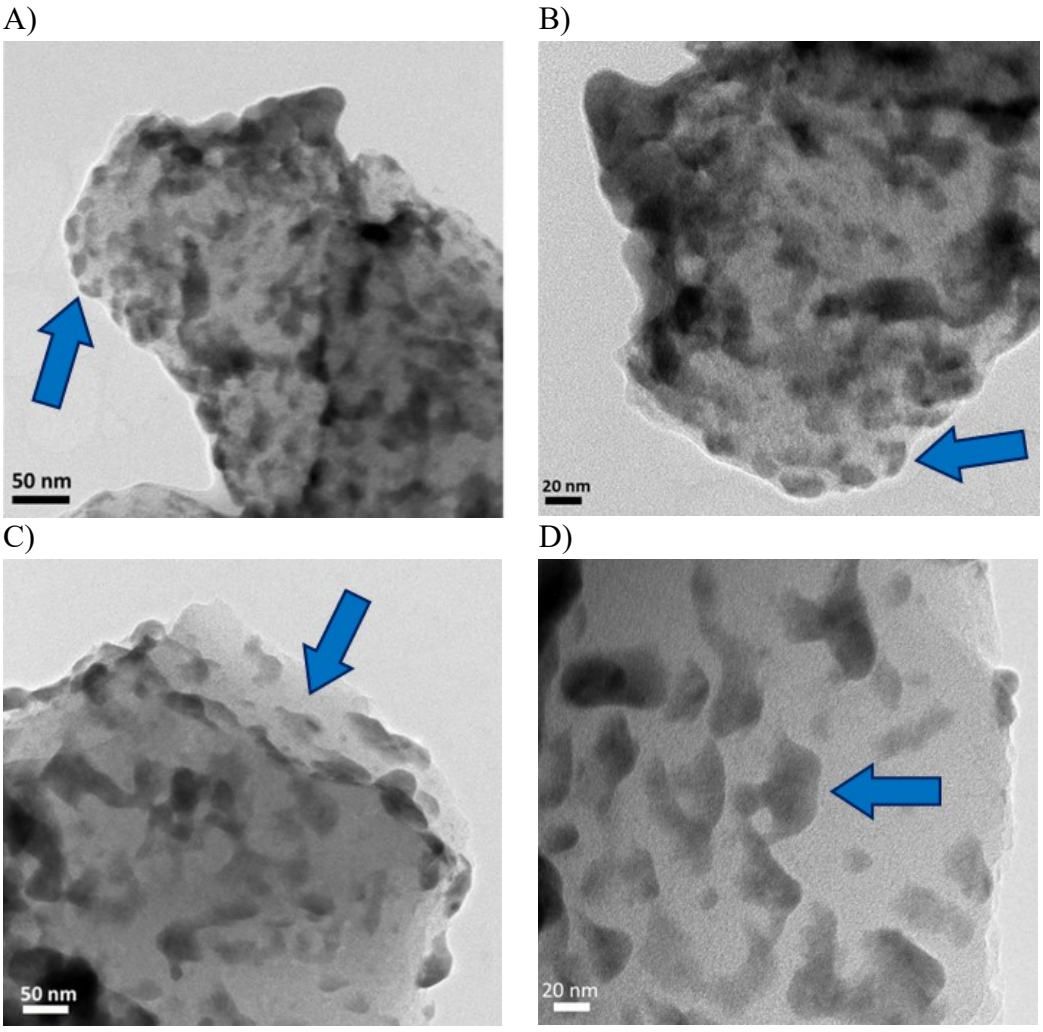

Figure S1. *A) and B) TEM images of YP50F + 10wt% Bi_2S_3. C) and D) TEM images of YP50F + 10wt% Bi_2S_3 + MPA with 50 nm scale and 20 nm scale. Arrows have been included to indicate the location of Bi_2S_3 NCs.*

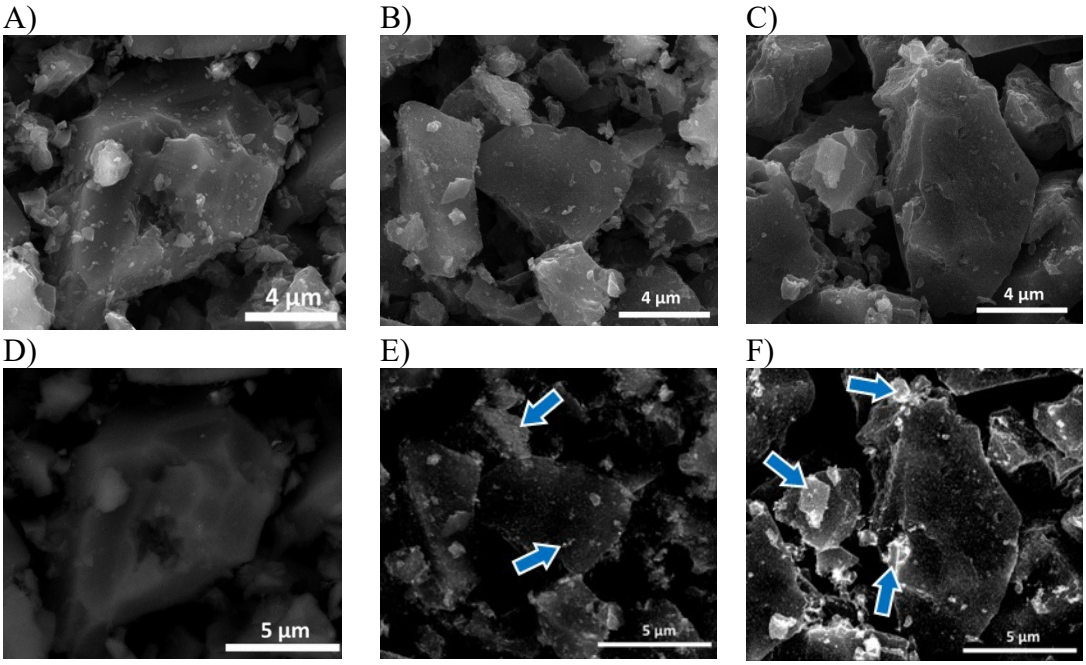

Figure S2. *SEM images with of A) YP50F, B) YP50F + 5wt% Bi_2S_3 and C) YP50F + 10wt% Bi_2S_3 with secondary electrons (SE) mode and with back scattered diffraction mode (BSED) (D, E, F respectively) in which heavier elements appear brighter and in our case is related to the presence of Bi_2S_3 nanocrystals (scale is 5 µm). Magnification is x20000. Arrows have been included to indicate the location of Bi_2S_3 NCs.*

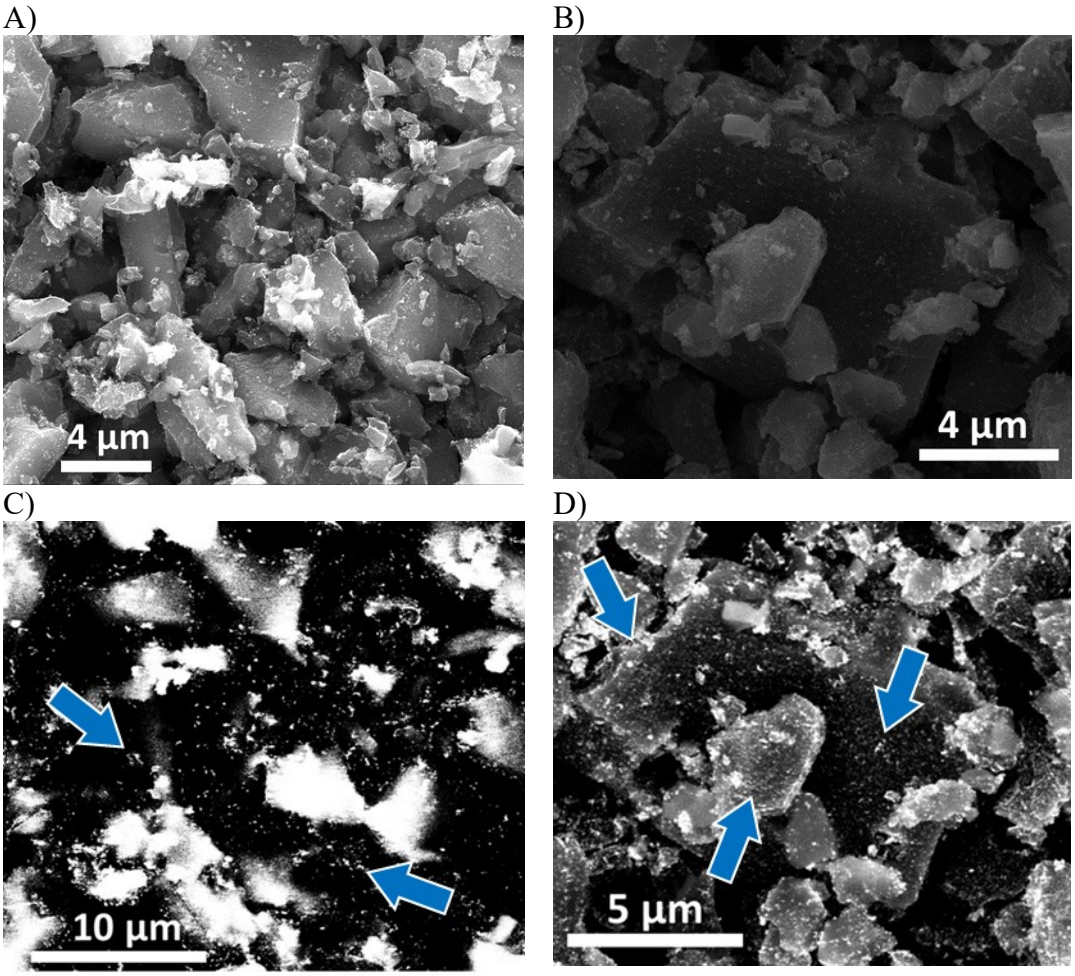

Figure S3. *SEM images of A) YP50F + 5wt% Bi_2S_3 + MPA and B) YP50F + 10wt% Bi_2S_3 + MPA in SE and in BSED mode (C and D respectively). Arrows have been included to indicate the location of Bi_2S_3 NCs.*

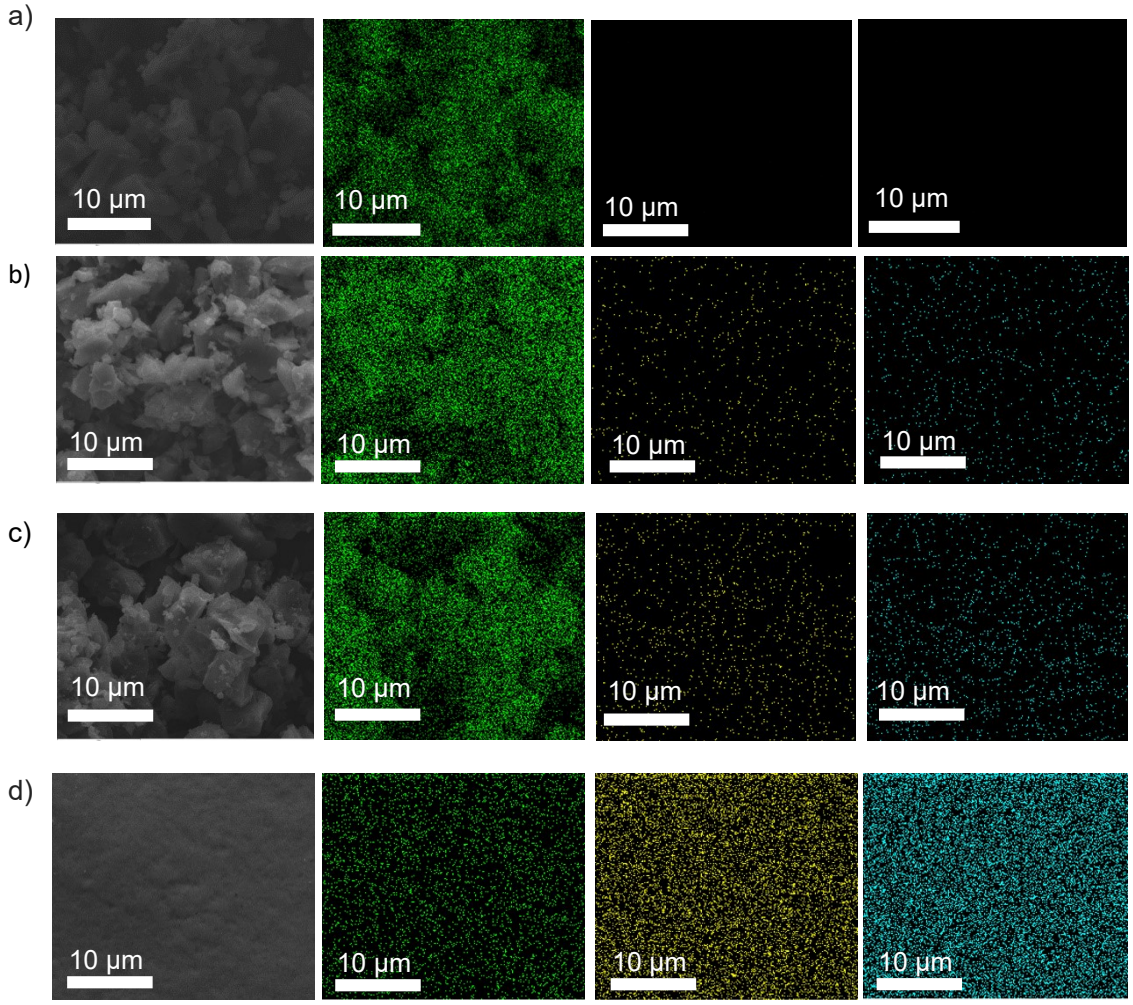

***Figure S4**. SEM-EDS elemental mapping of (a) YP50F, (b) YP50F + 5wt% Bi_2S_3, (c) YP50F + 10wt% Bi_2S_3, and (d) as-synthesized Bi_2S_3 NCs. C in green, S in yellow and Bi in blue.*

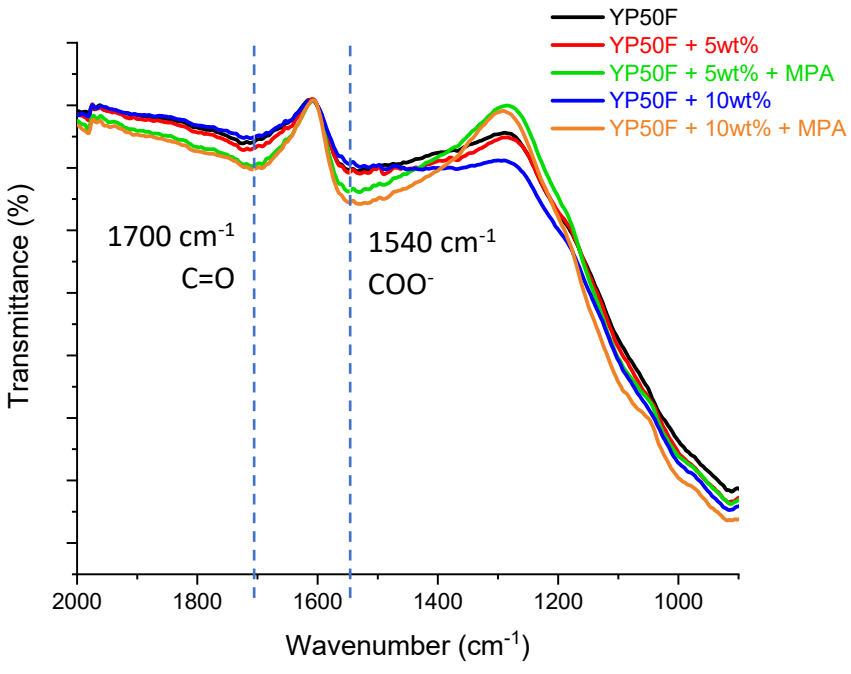

Figure S5. *FTIR spectra of YP50F (black), YP50F + 5wt% Bi_2S_3 (red), YP50F + 10wt% Bi_2S_3 (blue), YP50F + 5wt% Bi_2S_3 +MPA (green) and YP50F + 10wt% Bi_2S_3 + MPA (orange) after 250 scans, 4 cm^{-1} resolution, from 900 to 2000 cm^{-1}.*

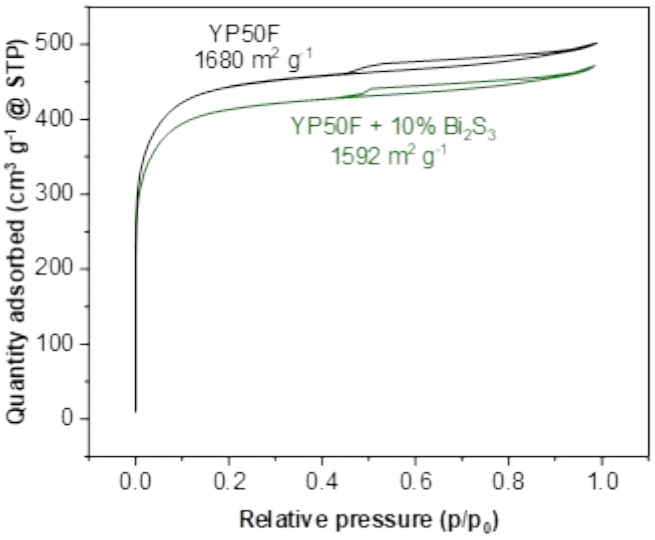

Figure S6. *Nitrogen adsorption/desorption isotherm at 77K to determine the surface area.*

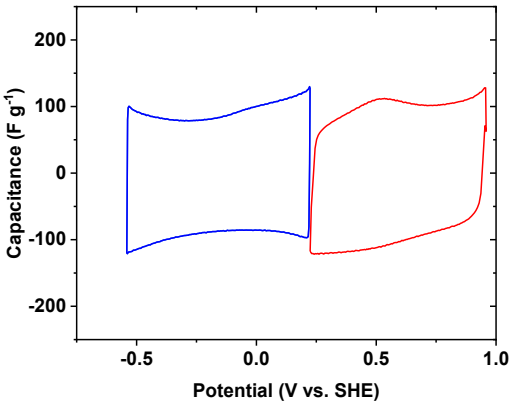

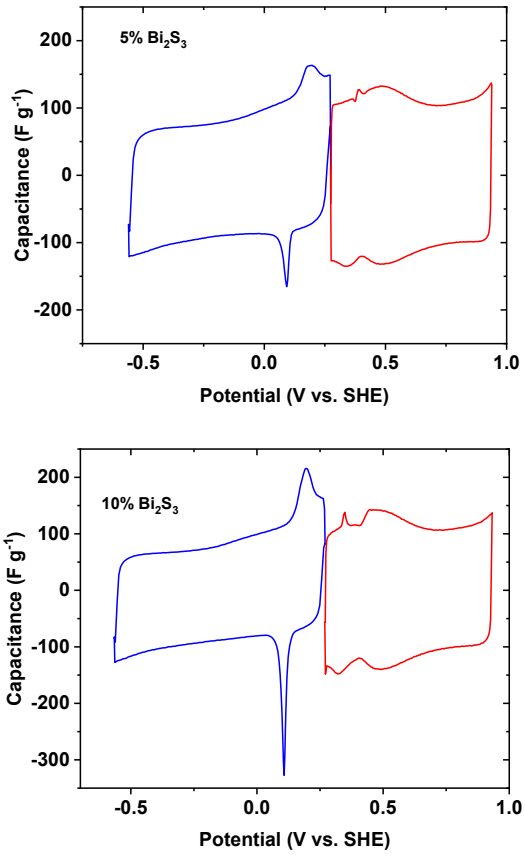

Figure S7 *Electrodes operation voltammetry in YP50F + Bi_2S_3 in 1 M Li_2SO_4 at 5 $mV \cdot s^{-1}$. Cell voltage 1.5 V.*

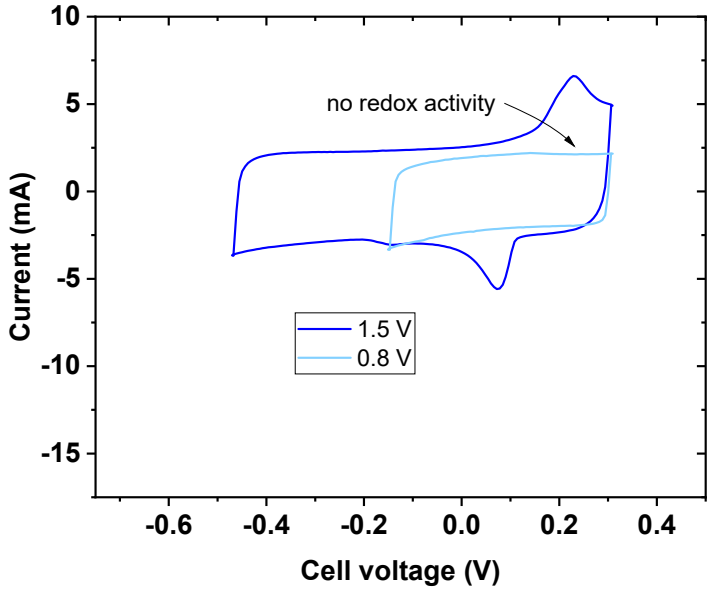

Figure S8 *Negative electrode operation voltammetry in YP50F + 10wt% Bi_2S_3 in 1 M Li_2SO_4 at 5 $mV \cdot s^{-1}$. Cell voltage 0.8V and 1.5 V.*

Table S1 *Elemental composition of pristine electrode containing 10wt% Bi_2S_3 and electrodes from the systems operating at different upper cell voltage limits 0.8 V and 1.5 V.*

Electrode	*N*	*C*	*H*	*S*
YP50F + Bi_2S_3 pristine	*0.4*	*85.7*	*1.0*	*0.6*
YP50F + Bi_2S_3 positive (1.5 V)	*0.0*	*82.6*	*1.2*	*0.6*
YP50F + Bi_2S_3 negative (1.5 V)	*0.6*	*85.9*	*1.0*	*0.1*
YP50F + Bi_2S_3 positive (0.8 V)	*0.3*	*82.9*	*1.0*	*0.9*
YP50F + Bi_2S_3 negative (0.8 V)	*0.5*	*85.9*	*1.0*	*0.3*

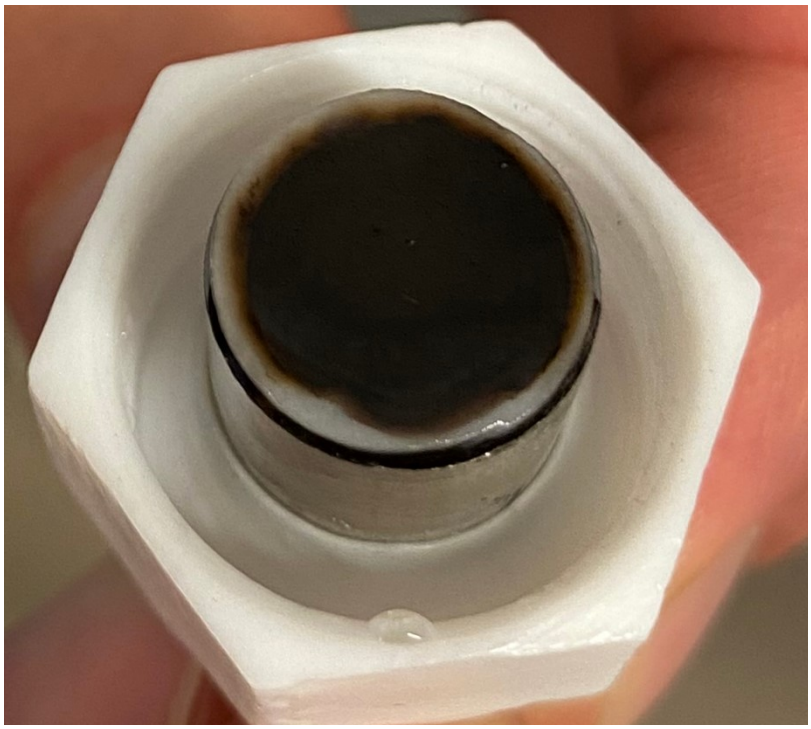

Figure S9 *Metallic deposition of bismuth on glass fiber separator of the cell YP50F + Bi_2S_3 in 1 M Li_2SO_4 at 1.5 V.*

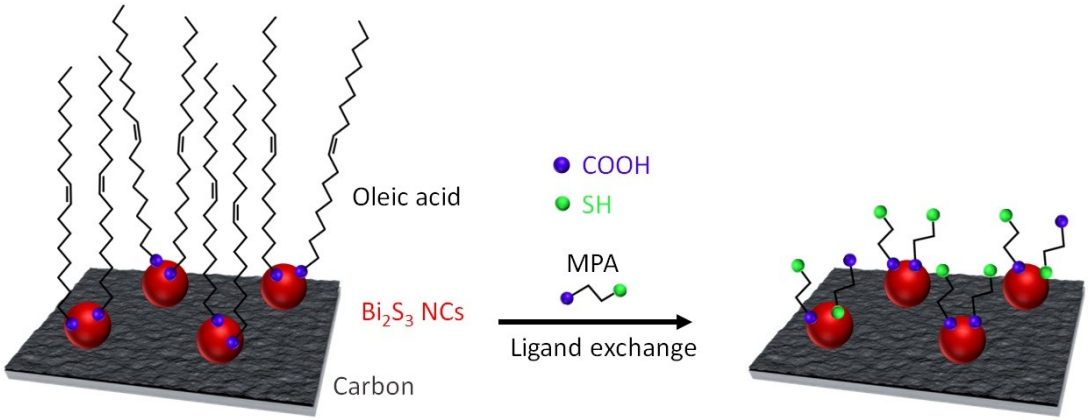

Figure S10 *Scheme of the 3-mercaptopropionic acid (MPA) ligand exchange treatment where MPA molecules substitute the stabilizing oleic acid chains on the surface of the Bi_2S_3 nanocrystals. Most of MPA molecules bond to the NCs through the carboxylic acid end. Blue spheres represent carboxylic acid groups and green spheres, thiol groups.*

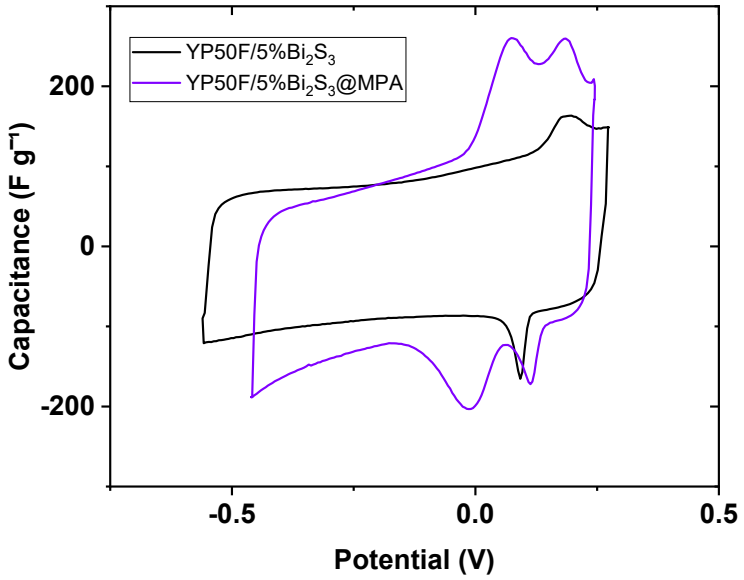

Figure S11 *Comparison of the negative electrode responses in 5wt% Bi_2S_3 and 5wt% Bi_2S_3 + MPA. (cell polarized to 1.5 V) in 1 M Li_2SO_4 at 2.5 $mV{\cdot}s^{-1}$.*

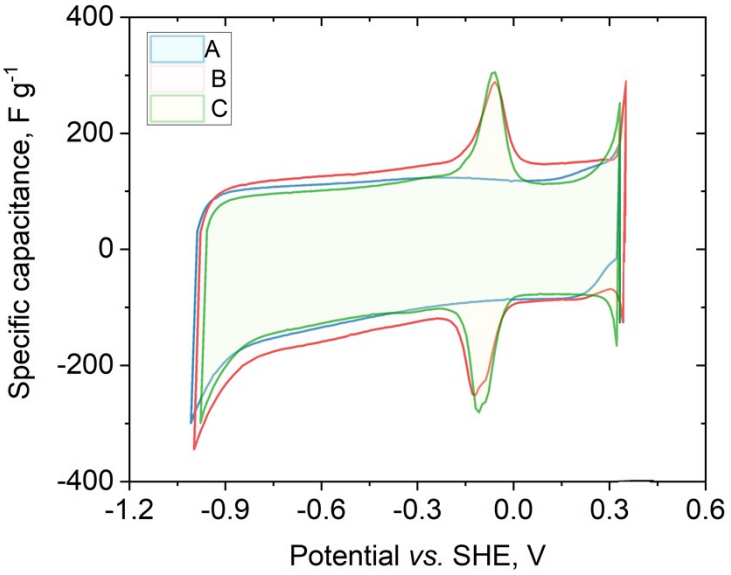

Figure S12 *Specific capacitances calculated from SPECS data of the negative electrode of YP50F (A), 5wt% Bi_2S_3 + MPA (B) and 5wt% Bi_2S_3 (C) in 1 mol L^{-1} NaI with 2:1 electrode mass ratio.*

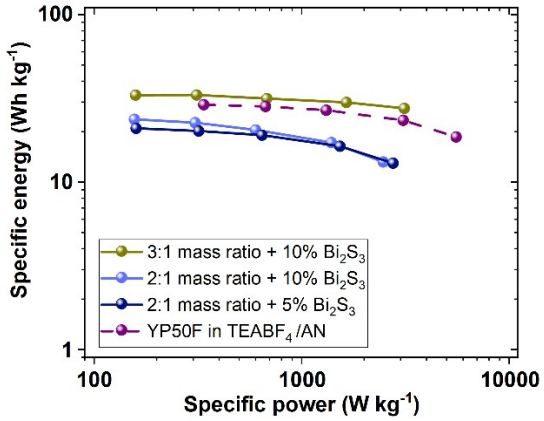

Figure S13 *Ragone plot for different negative-to-positive electrode mass ratios of the systems. Comparison with organic medium. Specific values expressed per mass of both electrodes.*

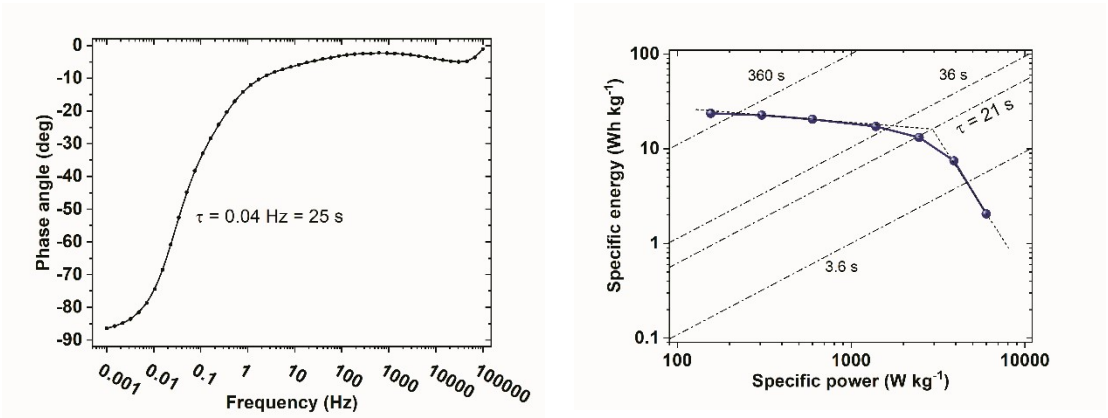

Figure S14 *Bode plot (ac) and Ragone plot (dc) in wide discharge rate spectrum to analytically determine RC time constant.*

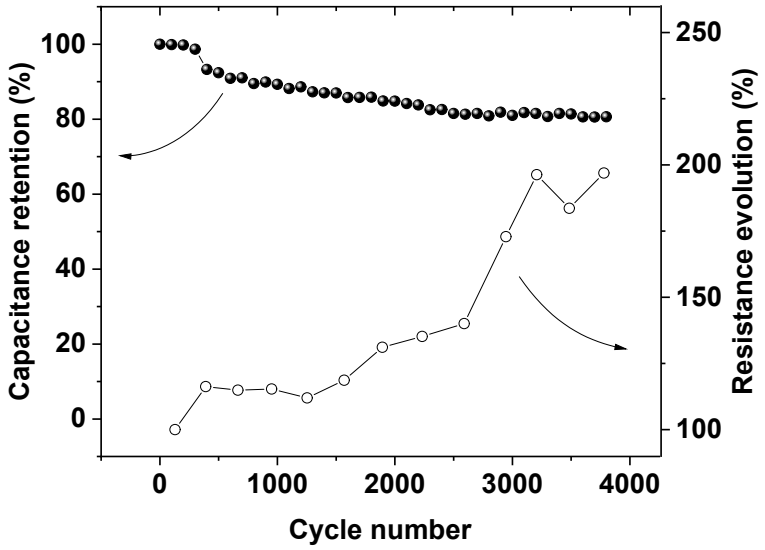

Figure S15 *Cyclability of the system (1 A g^{-1}) (-) YP50F + 10wt%Bi_2S_3 + MPA // YP50F (+) (1 mol L^{-1} NaI) $m_-:m_+$ = 2:1.*